QUANTITATIVE STUDY OF ITERATIVE RECONSTRUCTION ALGORITHMS OF SPECT/CT IN BONE SCAN: A CLINICAL AND PHANTOM STUDY

LAU LIK HAO

SCHOOL OF HEALTH SCIENCES
UNIVERSITI SAINS MALAYSIA

2024

QUANTITATIVE STUDY OF ITERATIVE RECONSTRUCTION ALGORITHMS OF SPECT/CT IN BONE SCAN: A CLINICAL AND PHANTOM STUDY

by

LAU LIK HAO

**Dissertation submitted in partial fulfilment of the requirements for the degree of
Bachelor of Health Science (Honours) (Medical Radiation)**

July 2024

CERTIFICATE

This is to certify that the dissertation entitled "QUANTITATIVE STUDY OF ITERATIVE RECONSTRUCTION ALGORITHMS OF SPECT/CT IN BONE SCAN: A CLINICAL AND PHANTOM STUDY" is the bona fide record of research work done by Mr LAU LIK HAO during the period from October 2023 to July 2024 under our supervision. We have read this dissertation and that in our opinion it conforms to acceptable standards of scholarly presentation and is fully adequate, in scope and quality, as a dissertation to be submitted in partial fulfillment for the degree of Bachelor of Health Science (Honours) (Medical Radiation).

Main supervisor,   Co-supervisor,

…………………………………   …………………………………...

Dr. Mohd Syahir bin Mansor   Dr. Mohammad Khairul Azhar Abdul Razab

University Lecturer   University Lecturer

Advanced Medical and Dental Institute   School of Health Sciences

Universiti Sains Malaysia   Universiti Sains Malaysia Health Campus

Bertam 13200 Kepala Batas   16150 Kubang Kerian

Penang, Malaysia.   Kelantan, Malaysia.

Date: July 2024   Date: July 2024

DECLARATION

I hereby declare that this dissertation is the result of my own investigations, except where otherwise stated and duly acknowledged. I also declare that it has not been previously or concurrently submitted as a whole for any other degrees at Universiti Sains Malaysia or other institutions. I grant Universiti Sains Malaysia the right to use the dissertation for teaching, research, and promotional purposes.

………………..

LAU LIK HAO

Date: July 2024

ACKNOWLEDGEMENT

TABLE OF CONTENTS

LIST OF TABLES

LIST OF FIGURES

LIST OF SYMBOLS

K_2HPO_4	Dipotassium hydrogen phosphate
^{18}F-NaF	Fluorine-18-sodium fluoride
^{99m}Tc-MDP	Technetium-99m methylene diphosphonate
^{99m}Tc	Technetium-99m
μ	Linear attenuation coefficient
ρ	Density
m	Mass
v	Volume
A	Actual activity of ^{99m}Tc source
A_0	Initial activity of 99mTc source
λ	Decay constant
t	Half life
$C_{measured}$	Measured mean activity concentration of the sphere or lesion
C_{true}	True activity concentration of the sphere
C_{VOI}	Mean activity concentration of the sphere or lesion
C_{BK}	Mean activity concentration of the background
σ_{BK}	Standard deviation of background counts
M_{BK}	Mean of the background counts
N	Noise

LIST OF ABBREVIATIONS

SPECT	Single photon emission computed tomography
CT	Computed tomography
RPC	Radiopharmaceutical
3D	Three-dimensional
PET	Positron emission tomography
MRI	Magnetic resonance imaging
2D	Two-dimensional
FBP	Filtered back projection
MLEM	Maximum-likelihood expectation-maximization
OSEM	Ordered-subsets expectation-maximization
SUV	Standardized uptake value
RC	Recovery coefficient
SNR	Signal-to-noise ratio
LEHR	Low energy-high resolution
EM	Expectation maximization
FOV	Field of view
CNR	Contrast-to-noise ratio
MMWF	Median modified Wiener filter
ASIR	Adaptive statistical iterative reconstruction
SSIM	Structural similarity
qSMART	Quasi-simultaneous multiplicative algebraic reconstruction technique

FWHM	Full width at half maximum
HUSM	Hospital Universiti Sains Malaysia
IEC	International Electrotechnical Commission
NEMA	National Electrical Manufacturers Association
TBR	Tumor-to-background ratio
SCF	Scatter weighting factor
VOI	Volume of interest
MLEM-CHANG	MLEM with Chang's attenuation correction method
OSEM-CHANG	OSEM with Chang's attenuation correction method
OSEM-CT	OSEM with CT based attenuation correction method
SPSS	Statistical Package for Social Sciences
PVE	Partial volume effect

LIST OF APPENDICES

KAJIAN KUANTITATIF ALGORITMA REKONSTRUKSI ITERATIF SPECT/CT DALAM PENGIMEJAN TULANG: KAJIAN KLINIKAL DAN FANTOM

ABSTRAK

Penggabungan tomografi pancaran foton tunggal (SPECT) dengan tomografi berkomputer (CT), bersama dengan kemajuan dalam algoritma rekonstruksi iteratif, meningkatkan kebolehlaksanaan kuantifikasi SPECT dalam pengimejan tulang secara signifikan. Kuantifikasi SPECT tulang membolehkan pengukuran tepat pengumpulan radioisotop dalam tumor tulang. Keupayaan ini membolehkan penilaian tepat mengenai kehadiran dan tahap keabnormalan tulang, seterusnya meningkatkan ketepatan diagnostik dalam pengimejan tulang. Kajian ini bertujuan untuk menilai kesan algoritma rekonstruksi iteratif dengan pelbagai kaedah pembetulan pemerosotan terhadap ketepatan kuantifikasi SPECT dan kualiti imej dalam pengimejan tulang dengan pelbagai bilangan iterasi dalam kajian fantom dan klinikal. Dalam kajian fantom, sfera-sfera fantom NEMA 2012/IEC 2008 diisi dengan campuran larutan K_2HPO_4 dan sumber ^{99m}Tc pada kepekatan 300 kBq/ml, manakala kawasan latar belakang hanya mengandungi sumber ^{99m}Tc pada kepekatan 30 kBq/ml, menetapkan nisbah tumor-ke-latar belakang (TBR) 10:1. Fantom tersebut menjalani imbasan tulang menggunakan protokol standard yang diterapkan di Hospital Universiti Sains Malaysia (HUSM). Dalam kajian klinikal, imej imbasan tulang pelvis yang mengandungi pelbagai tumor tulang diperoleh daripada stesen kerja Xeleris^{TM}. Kedua-dua imej fantom dan klinikal direkonstruksi menggunakan MLEM-CHANG, OSEM-CHANG, dan OSEM-CT, dengan pelbagai hasil darab iterasi (4, 8, 12, 16, dan 20 iterasi untuk MLEM; 40, 80, 120, 160, and 200 iterasi untuk OSEM). Analisis kuantitatif dari segi

kepekatan aktiviti, pekali pemulihan (RC), nilai pengambilan piawai (SUV), nisbah isyarat-ke-hingar (SNR), dan hingar dilakukan dengan menggunakan perisian Dosimetry Toolkit dan Q.Metrix. OSEM-CT (-73.3% hingga 6.7%) menunjukkan perbezaan peratusan terkecil antara kepekatan aktiviti yang diukur dan kepekatan aktiviti sebenar (300 kBq/ml) merentasi semua isipadu sfera dan bilangan iterasi berbanding MLEM-CHANG (-86.7% hingga -43.3%) dan OSEM-CHANG (-83.3% hingga -33.3%). Untuk semua algoritma, peningkatan bilangan iterasi meningkatkan RC, SUV, dan hingar, manakala SNR menurun. Dalam kajian fantom, tiada perbezaan yang signifikan dalam RC dan SNR antara pasangan algorithma (MLEM-CHANG vs OSEM-CHANG, MLEM-CHANG vs OSEM-CT, dan OSEM-CHANG vs OSEM-CT) merentasi bilangan iterasi yang berbeza (p>0.05), seperti diuji menggunakan ujian Kruskal-Wallis dengan pembetulan post-hoc Bonferroni. Dalam kajian klinikal, perbezaan yang signifikan dalam SUV dipaparkan antara MLEM-CHANG vs OSEM-CT dan OSEM-CHANG vs OSEM-CT pada semua bilangan iterasi (p<0.05). Seterusnya, SNR tumor dalam kajian klinikal menunjukkan perbezaan yang signifikan antara MLEM-CHANG dan OSEM-CT pada iterasi 8, 12, dan 16 (p < 0.05). Kesimpulannya, OSEM-CT menunjukkan ketepatan kepekatan aktiviti, RC, SUV, dan SNR yang lebih tinggi, serta hingar yang lebih rendah, berbanding OSEM-CHANG dan MLEM-CHANG. Oleh itu, OSEM-CT disyorkan untuk digunakan dalam pengimejan tulang bagi mencapai kuantifikasi SPECT yang tepat dan kualiti imej yang optimal.

QUANTITATIVE STUDY OF ITERATIVE RECONSTRUCTION ALGORITHMS OF SPECT/CT IN BONE SCAN: A CLINICAL AND PHANTOM STUDY

ABSTRACT

The integration of single photon emission computed tomography (SPECT) with computed tomography (CT), along with advancements in iterative image reconstruction algorithms, significantly enhances the feasibility of SPECT quantification in bone scan. Quantitative bone SPECT enables the precise measurement of radiotracer accumulation in bone lesions. This capability allows for the accurate assessments of the presence and extent of bone abnormalities, thereby improving diagnostic accuracy of bone scan. This study evaluates the impact of iterative reconstruction algorithms with various attenuation correction methods on SPECT quantification accuracy and image quality in bone scan across different iteration numbers in both phantom and clinical settings. In the phantom study, spheres in the NEMA 2012/ IEC 2008 phantom were filled with 300 kBq/ml of mixture of K_2HPO_4 solution and a ^{99m}Tc source, while the background region contained only 30 kBq/ml of ^{99m}Tc source, establishing a tumor-to-background ratio (TBR) of 10:1. The phantom underwent bone imaging using the standard protocol applied at Hospital Universiti Sains Malaysia (HUSM). In the clinical study, a pelvic bone scan image with multiple lesions was retrieved from the Xeleris^{TM} workstation. Both phantom and clinical images were reconstructed using MLEM-CHANG, OSEM-CHANG, and OSEM-CT, with varying iteration products (4, 8, 12, 16, and 20 iterations for MLEM; 40, 80, 120, 160, and 200 iterations for OSEM). Quantitative analysis of activity concentration, recovery coefficient (RC), standardized uptake value (SUV), signal-to-noise ratio (SNR), and noise

were performed using Dosimetry Toolkit and Q.Metrix software. OSEM-CT (-73.3% to 6.7%) demonstrated the smallest percentage difference between measured and actual activity concentration (300 kBq/ml) across all sphere volumes and iteration numbers compared to MLEM-CHANG (-86.7% to -43.3%) and OSEM-CHANG (-83.3% to -33.3%). For all algorithms, increasing the iteration numbers elevated RC, SUV, and noise, while SNR dropped. In the phantom study, there were no significant difference in RC and SNR among the algorithm pairs (MLEM-CHANG vs OSEM-CHANG, MLEM-CHANG vs OSEM-CT, and OSEM-CHANG vs OSEM-CT) across different iteration numbers ($p > 0.05$), as tested using the Kruskal-Wallis test with post-hoc Bonferroni's correction. In the clinical study, significant differences in SUV were displayed between MLEM-CHANG vs OSEM-CT and OSEM-CHANG vs OSEM-CT at all iteration numbers ($p < 0.05$). Additionally, the SNR of the lesions in clinical study showed significant differences between MLEM-CHANG and OSEM-CT at iterations of 8, 12 and 16 ($p < 0.05$). In summary, OSEM-CT illustrated higher activity concentration accuracy, RC, SUV, and SNR, along with lower noise level compared to OSEM-CHANG and MLEM-CHANG. Thus, OSEM-CT is recommended for accurate SPECT quantification and optimal image quality in bone scan.

CHAPTER 1

INTRODUCTION

1.1   Background of the Study

Nuclear medicine is an advanced branch of medicine that employs radioactive substances, referred to as radiopharmaceuticals (RPC) or radioactive tracers, to diagnose, stage, and treat different medical conditions, including cancer. Unlike traditional radiology, which focuses on anatomical imaging, nuclear medicine assesses the functional aspects of organs and tissues. Single photon emission computed tomography (SPECT) is a technique that is used in nuclear medicine imaging to obtain three-dimensional (3D) functional information about the physiological processes within the human body.

SPECT images provide limited anatomical information, leading to difficulty in identifying the exact location of the functional abnormalities. To overcome this, hybrid imaging systems combining SPECT with computed tomography (CT) were proposed in the early 2000s (Grosser et al., 2015). Modern hybrid SPECT/CT scanners integrate dual-headed SPECT with multi-slice CT systems (Cherry et al., 2012). In SPECT/CT imaging, SPECT and CT images are co-registered or fused, presenting both functional (SPECT) and anatomical (CT) information together within the same image frame (Ritt et al., 2014). According to Kinahan et al. (2003), hybrid systems improve attenuation correction by using patient-specific attenuation maps obtained from CT scans. Additionally, it has been valuable in correlating functional data derived from radionuclide images with anatomical details observed in CT scans. The images formed with detailed anatomical information permit the precise localization of functional disorders.

Furthermore, quantitative imaging was first utilized in positron emission tomography/computed tomography (PET/CT) applications and has since become the standard method for diagnostic evaluation in nuclear medicine imaging. Integration of SPECT with CT enhances the potential for SPECT quantification. Advancement in reconstruction algorithms have enabled the quantification of SPECT/CT by addressing partial volume resolution losses and scatter contamination of the main photon peak (Brady and Shulkin, 2019). These improvements allow for the conversion of pixel values (kBq/cts) to in vivo radioactivity concentrations (Bq/cm³). According to Bailey and Willowson (2013), SPECT is superior to PET due to the longer physical half-life of its radionuclide which align better with the biological half-life of physiological functions, and the easier availability of these radionuclide without the need for a cyclotron. Next, the wide variety of radiotracers available for SPECT imaging enables the evaluation of various clinical indications. The global availability and lower cost of SPECT/CT have further driven the adoption of SPECT quantification.

The attainment of absolute quantitation in ^{99m}Tc bone SPECT/CT is increasingly viable for diagnostic purposes and monitoring treatment outcomes (Miyaji et al., 2020). Precise absolute quantification of radiotracer distribution is imperative for dosimetry in personalized radionuclide therapy as it enhances the anticipation of therapy response, mitigate the risk of toxicity, and streamline treatment monitoring (Peters et al., 2019). Earlier investigations have demonstrated that the quantitative precision of SPECT imaging with ^{99m}Tc falls within a range of ± 10% (Ritt et al., 2011).

SPECT/CT is a powerful imaging instrument in bone scan. SPECT/CT can assess the suspected skeletal abnormalities, as it not only detects the radiotracer uptake in soft

tissue but also identifies the disease's extent and activity. Based on the study conducted by Rager et al. (2017), the number of ambiguous lesions detected by SPECT/ CT is lower than that in planar bone imaging due to its ability for accurate anatomic localization of the tumors. Additionally, SPECT/CT can offer significant findings in determining specific causes of lower back pain in comparison to magnetic resonance imaging (MRI) (Kato et al., 2019). SPECT imaging also has higher sensitivity in lesion detection than planar imaging. For instance, the presence of SPECT has increased the capability to detect avascular necrosis to 85% as opposed to the 55% sensitivity achieved by planar imaging (Katua et al., 2011). Importantly, there is no reduction of specificity from the sensitivity improvement.

The working principles of SPECT imaging involve gamma ray emission and detection. The patient is administrated with RPC, and the RPC will be absorbed by the specific organs. The detector heads will rotate around the patient and capture the photons emitted by the RPC. Multiple projections are performed from different angles during image acquisition. A sinogram, the two-dimensional (2D) matrix that encompasses all the projection data detected throughout the scan is obtained (Cherry et al., 2012). A row across the matrix displays the intensity for a single projection, whereas the consecutive rows indicate the subsequent projection angles. The computer will process the sinogram data to generate a 3D image that shows the tracer distribution within the patient's body (Cherry et al., 2012). The processing of the sinogram will involve the usage of image reconstruction and intricate mathematical algorithms.

SPECT performance is primarily assessed based on its sensitivity and image quality (Hoffmann et al., 2020). The choice of image reconstruction technique significantly affects

the resulting image quality (Yamamoto et al., 2008). There are two main types of image reconstruction algorithms being used in SPECT/CT imaging: analytic and iterative reconstruction algorithms. The analytic reconstruction algorithms include simple back projection and filtered back projection (FBP). Moreover, the most commonly used iterative reconstruction algorithms are maximum-likelihood expectation-maximization (MLEM) and ordered-subsets expectation-maximization (OSEM).

Analytic reconstruction approaches often employ simplified models of emission and detection processes, leading to the formation of streak artifacts and noise in the images (Zeraatkar et al., 2017). Contrarily, iterative reconstruction methods can integrate advanced models that take into account the statistical aspects of the emission process, as well as the factors such as attenuation, scatter, and detector response function during the image reconstruction. Hence, the images with less noise will be formed through the iterative reconstruction algorithms. Apart from that, FBP utilizes a low-pass filter to minimize image noise, however contributing to the loss of image spatial resolution. Iterative methods apply the weighting factors based on the noise variance and regularization techniques to regulate image noise (Zeng, 2018). Since the iterative approaches do not employ the low-pass filter, they are capable of decreasing image noise while preserving the image resolution. Due to the limitation of analytic image reconstruction techniques, especially FBP, iterative reconstruction methods have emerged as the preferred choice for SPECT image reconstruction (Rousset and Zaidi, 2006).

1.2   Problem Statement

Quantitative bone SPECT shows potential in aiding patient follow-up and facilitating the dose comparison between patients (Kangasmaa et al., 2021). It enhances bone SPECT image analysis by using standardized uptake value (SUV), hence eliminating bladder activity scaling issues. Factors like image reconstruction algorithms and iteration numbers significantly influence bone SPECT quantification (Peters et al., 2019). Achieving accurate SPECT quantification requires balancing high resolution for precise localization and delineation of volumes of interest (VOIs) with minimal noise for accurate activity concentration measurements. Additionally, attenuation correction during image reconstruction, compensating for photon attenuation by body tissues, further enhances SPECT quantification accuracy (Bailey and Willowson, 2014). Tissues with varying densities, such as bone and soft tissue, impact radioactivity detection due to difference in attenuation. Selecting appropriate image reconstruction algorithms and attenuation correction approaches is crucial for accurate SPECT quantification in bone scan. Therefore, a study is needed to assess the accuracy of activity concentration quantification among MLEM-CHANG, OSEM-CHANG, and OSEM-CT at different iteration numbers.

The most commonly used iterative image reconstruction methods in SPECT imaging are MLEM and OSEM. The fundamental distinction is that each MLEM image estimation update involves back and forward projection for all projection angles, whereas OSEM utilizes a subset of projection angles for each update. Hence, OSEM requires less time to complete an iteration than MLEM, making it more practicable in clinical applications. In terms of computational efficiency, OSEM outperforms MLEM by applying subset methods to minimize the computational burden for processing the entire dataset in

each iteration. Despite the wide employment of iterative reconstruction techniques in clinical practice, there is still a notable lack of studies investigating the performance disparities among different iterative reconstruction methods in bone scan in both phantom and clinical contexts.

Besides, variation in iteration numbers affects the performance of the image reconstruction algorithms. An increase in the number of iterations typically improves image resolution but simultaneously amplifies image noise (Kupitz et al., 2021). Thus, this study aims to quantitatively compare the performance of MLEM-CHANG, OSEM-CHANG, and OSEM-CT based on various imaging parameters (recovery coefficient (RC), standardized uptake value (SUV), signal-to-noise ratio (SNR), and noise) for bone scan images at different iteration numbers in both phantom and clinical settings.

1.3   Study Objective

1.3.1   General Objective

The aim of this study is to investigate the effect of the iterative reconstruction algorithms with various attenuation correction methods on the SPECT quantification accuracy and image quality in bone scan under varying iteration numbers.

1.3.2   Specific Objectives

1. To evaluate the quantitative accuracy of activity concentration and imaging parameters (recovery coefficient (RC), signal-to-noise ratio (SNR), and noise)

provided by bone SPECT imaging with various reconstruction algorithms (MLEM-CHANG, OSEM-CHANG, and OSEM-CT) across different iteration numbers in bone equivalent density solution within each sphere of the NEMA 2012/ IEC 2008 phantom.

2. To compare the imaging parameters (standardized uptake value (SUV), signal-to-noise ratio (SNR), and noise) of the bone scan with various reconstruction algorithms (MLEM-CHANG, OSEM-CHANG, and OSEM-CT) across different iteration numbers in the clinical study.

1.4   Study Hypothesis

1.4.1   Null Hypothesis

1. There is no significant difference between the imaging parameters (recovery coefficient (RC) and signal-to-noise ratio (SNR)) provided by bone SPECT imaging with various reconstruction algorithms (MLEM-CHANG, OSEM-CHANG, and OSEM-CT) across different iteration numbers in bone equivalent density solution within each sphere of the NEMA 2012/ IEC 2008 phantom.

2. There is no significant difference between the imaging parameters (standardized uptake value (SUV), and signal-to-noise ratio (SNR)) of the bone scan with various reconstruction algorithms (MLEM-CHANG, OSEM-CHANG, and OSEM-CT) across different iteration numbers in the clinical study.

1.4.2 Alternative Hypothesis

1. There is a significant difference between the imaging parameters (recovery coefficient (RC) and signal-to-noise ratio (SNR)) provided by bone SPECT imaging with various reconstruction algorithms (MLEM-CHANG, OSEM-CHANG, and OSEM-CT) across different iteration numbers in bone equivalent density solution within each sphere of the NEMA 2012/ IEC 2008 phantom.

2. There is a significant difference between the imaging parameters (standardized uptake value (SUV) and signal-to-noise ratio (SNR)) of the bone scan with various reconstruction algorithms (MLEM-CHANG, OSEM-CHANG, and OSEM-CT) across different iteration numbers in the clinical study.

1.5 Significance of the Study

This study can contribute to the selection of the most appropriate iterative reconstruction algorithms, specifically MLEM-CHANG, OSEM-CHANG, and OSEM-CT for bone scan using SPECT/CT. These algorithms play a vital role in reconstructing images from the raw data acquired during the scanning process. The choice of reconstruction algorithm can significantly impact the diagnostic accuracy of bone scan in clinical practice. By comparing these commonly employed algorithms, their respective strengths and weaknesses can be discovered, offering important information to practitioners regarding the preference and implementation of the preeminent algorithm in the daily clinical procedures. It is crucial to comprehend the performance of these algorithms in order to enhance the image quality and minimize the artifacts. Thus, physicians can have a better

detection and characterization of skeletal abnormalities, resulting in improved diagnostic outcomes.

Besides, this study serves as a valuable resource for the researchers to gain insights into the performance disparities of these algorithms under different conditions, particularly with various number of iterations. Hence, this information allows the determination of the optimal imaging parameters for bone scan. In addition, the accuracy of the bone SPECT quantification can be improved due to the selection of optimal iteration numbers and appropriate image reconstruction algorithms, ultimately enhancing the diagnostic precision of bone metastases.

CHAPTER 2

LITERATURE REVIEW

2.1   Effectiveness of SPECT/CT in Bone Scan

Previously, spot views or whole-body planar images were obtained for bone scan due to its ability to detect osseous lesions, making it a commonly utilized screening instrument for staging cancerous conditions (Kuwert, 2014). In the late 1980s, single photon emission computed tomography (SPECT), a modality that enables three-dimensional visualization of radioactivity distribution in human body, replaced planar imaging. This advancement significantly enhanced the diagnostic accuracy of skeletal scans, enabling improved localization of regions showing abnormal tracer uptake. However, the precision of bone scans remained restricted because of the spatial resolution constraints of skeletal SPECT, which typically range from approximately 8 to 10 mm in the reconstructed images (Even-Sapir, 2005). Lately, the hybrid system combining a SPECT camera with a CT scanner was introduced. Compared to SPECT imaging alone, SPECT/CT allows more accurate localization of pathological tracer uptake, identification of gross morphological abnormalities through CT diagnosis, and attenuation correction of reconstructed images (Kuwert, 2014).

SPECT/CT demonstrates its effectiveness in bone scans by improving the diagnostic accuracy of bone lesions. Horger et al. (2004) conducted a study involving 47 patients with 104 ambiguous lesions identified on bone scans, using histological confirmation or long-term follow-up as the benchmark. In this study, SPECT/CT achieved an accurate diagnosis in 85% of cases, notably by delineating the underlying characteristics

of focal areas displaying heightened uptake in the spine, rib cage, skull, and pelvis. Römer et al. (2006) had discovered that 92% of successful classifications of abnormal tracer uptake in 44 patients with 52 indeterminate bone lesions through SPECT/CT. Ndlovu et al. (2010) showed that the detection accuracy of bone diseases (malignant or benign) with SPECT/CT (92%) is higher than with SPECT alone (67%) when compared to the gold standard of their study, which is diagnostic radiology (radiograph, CT, or MRI).

2.2 SPECT Quantification in Bone Scan

Quantitative SPECT has been introduced for many years, but its application remains limited. A few methods based on quantitative SPECT, primarily in dosimetry after radionuclide therapy, have gained clinical acceptance (Kuwert, 2014). Quantitative bone SPECT may simplify the detection of the super-scan phenomenon, as there is no requirement to correlate bone uptake with kidney uptake (Love et al., 2003). Its limited application may be due to the inferior spatial resolution of SPECT/CT compared to PET/CT, leading to degraded quantitative performance. For instance, quantitative bone SPECT is rarely used in clinical setting as until now the distinction between lesions and normal bone tissue is primarily relied on visual diagnosis (Qi et al., 2021). Quantitative positron emission tomography (PET) bone imaging utilizing fluorine-18-sodium fluoride (^{18}F-NaF) is recognized for its probable clinical benefit. Nevertheless, ^{18}F-NaF PET/CT is costly and not widely available. The advancement of SPECT/CT technology has facilitated quantitative analysis of bone scan using Technetium-99m methylene diphosphonate (^{99m}Tc-MDP), a commonly used radiotracer in bone scan. SPECT quantitative assessment of bone scan demonstrated strong consensus among the observers (Beck et al., 2016). Arvola et al.

(2019) discovered that a significant correlation between standardized uptake value (SUV) acquired from SPECT images of bone metastases of breast and prostate cancer with SUV attained from PET images, indicating the capability of SPECT quantification utilizing SUV in bone imaging.

SPECT quantification accuracy presents challenges due to its reliance on various factors, such as the mandatory use of a collimator, differing detector trajectories, and the necessity for more intricate scatter and attenuation corrections compared to PET (Bailey and Willowson, 2014). In addition, the reconstruction algorithm and its parameters significantly influence the SPECT quantification (Peters et al., 2019). Recent advancements in photon attenuation and scatter corrections, collimator modelling, and 3D reconstruction, which include resolution recovery and noise regulation, have enhanced reconstruction approaches, thus permitting absolute SPECT quantification (Collarino et al., 2018). Moreover, the implementation of attenuation and scatter correction approaches is crucial for precise SPECT quantitative analysis. Bailey and Willowson (2013) reported that employing CT-based attenuation correction in SPECT reconstruction led to a quantification accuracy within 10%. Additionally, the choice of collimator significantly influences quantification accuracy due to the trade-off between spatial resolution and detector efficiency. Optimal SPECT quantification is achieved through data acquisition using an appropriate collimator type. The selection of collimator type depends heavily on the energy of the emitted photons, with the low energy-high resolution (LEHR) collimator commonly used for low-energy (^{99m}Tc) imaging. Narrowing the photopeak energy window and increasing the discriminator cut-off have been shown to enhance SPECT quantification accuracy (Ritt et al., 2011). Accurate SPECT quantification requires the balance between

the spatial resolution and noise. Inadequate spatial resolution can affect the radiotracer distribution measurement in small lesions due to blurring and partial volume effect (PVE) (Meechai et al., 2015). High levels of noise reduce the signal-to-noise ratio (SNR), making it challenging to distinguish radiotracer uptake from background noise (Kupitz et al., 2021). Thus, it may result in overestimation or underestimation of actual activity concentration.

2.3   Image Reconstruction Algorithms Used in SPECT/CT

In general, there are two types of image reconstruction algorithms used in SPECT/CT which are analytic and iterative reconstruction algorithms. The most commonly employed analytic reconstruction algorithm is filtered back projection (FBP) due to its straightforwardness, rapidity, and computational efficiency (Groch and Erwin, 2000). The images can be acquired in a short period of time as the image reconstruction process is easier as compared to the iterative approaches (Seret and Forthomme, 2009). It involves two primary steps: data filtering and back projection of the filtered data. The back projection occurs in the spatial domain, whereas the data filtration takes place in the frequency domain (Lyra and Ploussi, 2011). In 2D acquisition, each row of projections illustrates the addition of all counts along a straight line traversing the depth of the imaged object. The back projection process reallocates the number of counts detected at each specific point back along the lines where they were initially captured (Lyra and Ploussi, 2011). This process repeats for all pixels and angles. The restricted number of projection sets leads to the formation of star artifacts and image blurring. To mitigate these issues, the projections undergo filtration before being back projected onto the image matrix (Kim and Lee, 2023). However, the application of filter such as ramp, Butterworth, and Hanning

filters will increase the statistical noise and eventually deteriorate the image quality of the reconstructed images (Zeng, 2012). The FBP technique does not work well in generating images with higher region distinction, especially when dealing with incomplete data sampling (Winz et al., 2012). Besides, FBP does not have sufficient models to account for attenuation, scatter and collimator blurring artefacts. Thus, the iterative reconstruction technique with scatter and attenuation corrections has replaced the FBP method (Ritt et al., 2011).

In addition, the iterative reconstruction algorithm is based on statistical principles. It relies on the estimation of the real possibility of detecting a specific quantity of radioactivity at a given location within the imaging system at each particular point in every projection (Groch and Erwin, 2000). Firstly, it begins with an initial estimate of the image. Often, the initial estimation is quite basic, such as assuming a uniform distribution of activity (Lyra and Ploussi, 2011). The initial estimate is then forward projected to generate a set of projection data. These projections are compared to the estimated data, and any disparities are determined to obtain the pixel value correction. The correction values will then be utilized to update the estimated images (Bruyant, 2002). This iterative process continues until the discrepancies between calculated and measured data fall below a predefined threshold. Hence, it is possible to reduce the inaccuracies in the calculated values. Expectation maximization (EM) – based technique is the prevalently utilized iterative reconstruction approach. Examples of EM-based techniques include maximum-likelihood expectation-maximization (MLEM) and ordered-subsets expectation-maximization (OSEM). In OSEM, the initial image is updated after processing each subset of projections, whereas in MLEM, the image is only updated after all projections have been

processed (Ljungberg and Pretorius, 2018). OSEM is widely employed as compared to other EM-based algorithms as it enhances the SPECT/CT performances through the adjustment of iteration and subset numbers (Katua et al., 2011). According to Knoll et al. (2012), MLEM is deemed unsuitable to be applied in clinical settings due to its requirement for regularization and extended processing time. In contrast, OSEM, an accelerated version of MLEM, divides the projection sets into subsets, rendering it more practicable in clinical use.

2.4   Factors Affecting Quality of Images Reconstructed Using Image Reconstruction Algorithm

There are several factors that will influence the images reconstructed using image reconstruction algorithm. First of all, the selection of different attenuation correction approaches, such as Chang's method, radionuclide transmission-based attenuation correction method, and x-ray CT-based attenuation correction method, are among the primary elements altering image quality. Chang's method assumes a uniform linear attenuation coefficient (μ) across all the tissues (Nakamura et al., 2015). In other words, a constant μ value will be applied uniformly throughout all pixels in the attenuation map. This method produces satisfactory outcomes when employ in brain and abdomen imaging as the assumption of a constant μ value is reasonable due to the minimal presence of bone and air spaces (Cherry et al., 2012). However, its efficacy diminishes when imaging the thorax or pelvic region, where the substantial presence of lungs and bone can lead to notable inaccuracies. Furthermore, the radionuclide transmission-based attenuation correction method is performed by using an external radiation source to obtain transmission profile,

which can then be utilized for reconstructing cross-sectional images representing the μ value of tissue, commonly known as an attenuation map. Radionuclides such as gadolinium- 153, cobalt-57, barium-133, americium-241, and cerium-139 are example of transmission sources that are used in this technique (Cherry et al., 2012). To generate an attenuation map, two distinct scans are conducted using the transmission source. The initial scan, referred to as the blank or reference scan, is performed without any object present in the field of view (FOV) of the SPECT camera. Following this, the transmission scan, involving the object of interest within the FOV, is acquired. The transmission scan exhibits relatively high levels of noise, which can propagate to the emission scan and subsequently deteriorate the overall image quality further (Lee et al., 2016). The image quality produced by this method is inferior compared to x-ray CT-based method due to the restricted SPECT camera resolution and the low photon flux employed in capturing the transmission images (Cherry et al., 2012). Moreover, the x-ray CT-based attenuation correction method involves the conversion of pixel intensity or CT number based on Hounsfield Unit (HU) into μ value at the photon emission energy of radionuclide utilized, in order to generate an attenuation map. The attenuation map obtained shows superior spatial resolution and reduced noise level when contrasted with the attenuation map formed using the radionuclide transmission method (Lee et al., 2016). Among these attenuation corrections approaches, x-ray CT-based method results in the best quality of image.

Other than that, the selection of iteration and subset numbers significantly impacts the quality of the reconstructed images. According to the study conducted by Usman et al. (2016), the image of the anthropomorphic torso phantom with liver insert (containing a syringe sphere to mimic the liver tumor) was reconstructed using constant subsets (10

subsets) but varying iterations (2, 3, 4, 5, 6, 7, 8, 9, and 10 iterations). The contrast-to-noise ratio (CNR) increased from 3.71 to 3.89 between the 2nd iteration and the 4th iteration, but then declined to 2.01 from the 5th iteration to the 10th iteration. As the number of iterations increases, the noise level in the reconstructed images tend to rise, thereby reducing the CNR (Usman et al., 2016). Alqahtani et al. (2022) revealed that the image noise escalated from 7.84% to 10.17% when the iteration numbers rose from 4 to 24 iterations. With a high number of subsets, each subset becomes smaller, thereby reducing tomographic and statistical information within each subset (Morey and Kadrmas, 2013). Consequently, this loss of information can manifest as noise structures and artifacts in the final image. Morey and Kadrmas (2013) also discovered that the overall performance in lesion detection decreased with an increase in the number of subsets. This decline was moderate up to approximately 12–14 subsets, beyond which it became increasingly steep. Therefore, the appropriate iteration and subset numbers should be selected to produce good quality images. To illustrate, Trevisan et al. (2020) demonstrated that the highest quality image was achieved using 3 iterations and 8 subsets for brain scan, enabling clearer distinction between the putamen and the head of the caudate nucleus.

2.5 Comparison between the Performance of Various Image Reconstruction Algorithms

Several studies had concluded that iterative reconstruction algorithm is more superior than analytic reconstruction algorithm in reconstructing the images (Kim et al., 2021; Trevisan et al., 2020; Grosser et al., 2019; Zeng, 2018; Sowa-Staszczak et al., 2013; Arosio et al., 2011; Singh et al., 2010). According to Kim et al. (2021), they had discovered

that OSEM had 37.7% higher signal-to-noise ratio (SNR) and 25.9% higher contrast-to-noise ratio (CNR) than FBP. Kim et al. (2021) also concluded that the application of median modified Wiener filter (MMWF) will improve the image quality of brain SPECT imaging. The average SNR and CNR of OSEM and MLEM with MMWF were 35.9% and 17.1% greater, respectively, than those without MMWF. Trevisan et al. (2020) revealed that OSEM shown better differentiation between the putamen and the caudate nucleus than FBP, making it an invaluable tool for brain imaging. Both research performed by Grosser et al. (2019) and Singh et al. (2010) showed significantly lower noise level of image reconstructed using adaptive statistical iterative reconstruction (ASIR) as compared to FBP. MLEM illustrated lower normalized noise standard deviation (0.0277) than windowed FBP (0.0286) when the images were displayed with the same lesion contrast (Zeng, 2018). Based on the study conducted by Sowa-Staszczak et al. (2013), the lesion to noise ratio in OSEM was 1.5 times greater than in FBP for lesions located both within and outside the liver. The image contrast of OSEM (77%) was better than FBP (70%) (Arosio et al., 2011).

Apart from that, numerous researchers had conducted the studies between the newly developed and the existing reconstruction algorithm (Kim and Lee, 2023; Zeraatkar et al., 2017; Knoll et al., 2012). The reconstruction algorithm developed by Kim and Lee (2023) using the adaptive non-blind deconvolution with a structural similarity (SSIM) index in comparison with FBP and OSEM. The newly developed algorithm had average CNR values that were 2.76 times greater than FBP but 2.76 times smaller than OSEM. The quasi-simultaneous multiplicative algebraic reconstruction technique (qSMART) was proposed by Zeraatkar et al. (2017) to be applied in PERSPECT, a desktop open-gantry system specifically for tiny animals or tiny human's organ imaging. The contrast-to-noise ratio

(CNR) in the image reconstructed with qSMART (12.3) after 10 iterations was lower than OSEM (13.4) but higher than MLEM (10.8). After 3 iterations, qSMART (22% non-uniformity) had poorer image uniformity compared to MLEM (18% non-uniformity) and OSEM (14% non-uniformity) (Zeraatkar et al., 2017). According to Knoll et al. (2012), the advanced algorithms proposed by GE's Evolution, Philips Astonish, and Siemens Flash3D indicated 17 – 19% of spatial resolution improvement than FBP algorithm. Using the same reconstruction parameters (5 iterations and 15 subsets), GE's Evolution (7.9 mm FWHM) was found to have better spatial resolution than OSEM (9.4 mm FWHM).

CHAPTER 3

METHODOLOGY

3.1   Materials

The study was conducted at the Nuclear Medicine Department, Hospital Universiti Sains Malaysia (HUSM). The necessary equipment for performing this study included the GE Discovery NM/CT 670 Pro SPECT/CT machine, NEMA 2012/ IEC 2008 phantom, dipotassium hydrogen phosphate (K_2HPO_4) powder, technetium-99m (^{99m}Tc) source, Atomlab^{TM} 500 dose calibrator, hot plate and magnetic stirrer, analytical balance scale, beaker, centrifuge tube, 20 cc syringe, plastic tube, and Xeleris^{TM} workstation.

3.1.1   GE Discovery NM/CT 670 Pro SPECT/CT Machine

The SPECT/CT machine utilized in this study is Discovery NM/CT 670 Pro, manufactured by GE HealthCare as shown in Figure 3.1. This hybrid imaging system consists of dual-detector and free-geometry nuclear imaging camera equipped with sophisticated all-digital Elite NXT detector technology. This modality features a 70 cm wide-bore gantry that merges a slender NM gantry with a CT compact design. Data acquisition can be conducted in various imaging modes including static, dynamic, multi-gated, whole body planar and SPECT, as well as gated planar and SPECT. The acquisition station is linked with the Xeleris^{TM} workstation and outstanding Optima CT540 system. The Optima CT540 incorporates a 16-slice CT configuration with short-geometry along with Performix Ultra X-Ray Tube, boasting a tube anode heat storage capacity of 6.3 MHU and a maximum power of 53.2 kW.

Figure 3.1: GE Discovery NM/CT 670 Pro SPECT/CT machine.

3.1.2 NEMA 2012/ IEC 2008 Phantom

The NEMA 2012/ IEC 2008 phantom comprises a body phantom, a lung insert, and an insert featuring six spheres with varying sizes as presented in Figure 3.2. It adheres to the guidelines set by the International Electrotechnical Commission (IEC) and has been adapted by the National Electrical manufacturers Association (NEMA). The phantom descriptions are tabulated in Table 3.1. For this study, the fillable compartments of the phantom are loaded with diluted ^{99m}Tc source, possessing activity concentrations of 300 kBq/ml for the spheres and 30 kBq/ml for the D-shaped fillable cylinder in order to establish a tumor-to-background ratio (TBR) of 10:1.

Figure 3.2: NEMA 2012/ IEC 2008 phantom.

Table 3.1: NEMA 2012/ IEC 2008 phantom specifications.

NEMA 2012/ IEC 2008 Phantom Specifications	
Dimension	24.1 cm × 30.5 cm × 24.1 cm (height × width × depth)
Interior length	18 cm
Weight	4.9 kg
Fillable glass spheres	Diameters of 10 mm, 13 mm, 17 mm, 22 mm, 28 mm, and 37 mm Corresponding volume of 0.52 ml, 1.15 ml, 2.57 ml, 5.58 ml, 11.49 ml, and 26.52 ml
D-shaped fillable cylinder	Volume of 9700 ml
Cylindrical-shaped lung insert	Diameter of 50 mm

3.1.3 Dipotassium Hydrogen Phosphate (K₂HPO₄) Powder

Dipotassium hydrogen phosphate (K_2HPO_4) powder is a potassium salt derived from phosphoric acid and potassium chloride as demonstrated in Figure 3.3. It serves as a buffer and is categorized as both a potassium salt and an inorganic phosphate. It has a molar mass of 174.18 g/mol and pH value of 8.5 to 9.6. The selection of this chemical powder for this study is based on its bone-equivalent properties, which allow it to effectively simulate the characteristics of pelvic bone. The powder form is chosen as it facilitates rapid dissolution in saline water during the preparation of the K_2HPO_4 solution.
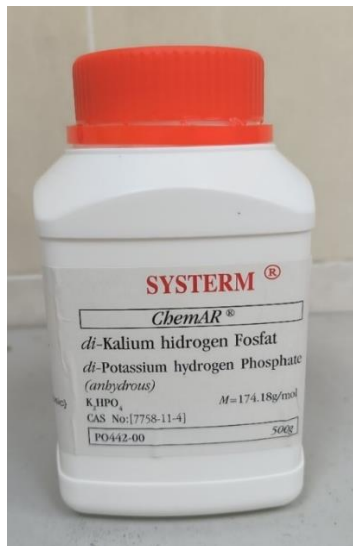

Figure 3.3: Dipotassium hydrogen phosphate (K_2HPO_4) powder.

3.1.4 Technetium-99m (^{99m}Tc) Source

Technetium-99m (^{99m}Tc) source is a widely used radioisotope in nuclear imaging such as bone scans, thyroid scans, renal imaging, and myocardial perfusion imaging as exhibited in Figure 3.4. It emits gamma rays with a photon energy of 140 keV and possesses a half-life of 6 hours. It can be obtained through the elution process from ^{99m}Tc generator.

In this study, the tumor-to-background ratio (TBR) of 10:1 was employed based on the specific activity concentrations of 300 kBq/ml for spheres and 30 kBq/ml for background. The total activity of the ^{99m}Tc source prepared was 373293 kBq. Specifically, 33633 kBq of the ^{99m}Tc source was allocated for the spheres while 339660 kBq was designated for the background. The ^{99m}Tc source for the spheres was diluted with tap water in a 100 ml beaker before being filled into the spheres.

Figure 3.4: Technetium-99m (^{99m}Tc) source.

3.1.5   Atomlab^{TM} 500 Dose Calibrator

Atomlab^{TM} 500 dose calibrator offers rapid and accurate measurements of radionuclide activity, effortlessly meeting stringent regulatory standards as revealed in Figure 3.5. It incorporates a low-pressure ionization chamber, an electrometer with exceptional linearity, and an auto-ranging color touch-screen display. It employs a pressurized detector filled with argon gas to determine the activity of a radionuclide source with a known isotope. It, designed as a well-type ionization chamber, can accurately